Comparison of well-mixed and multiple representative interactive flamelet approaches for Diesel spray combustion modelling

G. D'Errico[a*], T. Lucchini[a], F. Contino[b], M. Jangi[c], X-S. Bai[c]

[a]*Department of Energy, Politecnico di Milano, I-20156 Milan, Italy*; [b]*Department of Mechanical Engineering, Vrije Universiteit Brussel, B-1050 Brussels, Belgium*;

[c]*Department of Energy Sciences, Faculty of Engineering, Lund University, SE-221 00 Lund, Sweden*

1. Introduction

Diesel combustion modeling is a very challenging task due to the complex interplay of turbulence and chemistry which determines auto-ignition, flame structure, fuel oxidation, local quenching and pollutant formation. Despite the fact that each of these aspects has been matter of investigation for decades, a deeper understanding of many fundamental phenomena is still needed together with the achievement of time efficient CFD tools which can support the design of the next generation Diesel and HCCI engines. Recently, to reach such objectives, the Engine Combustion Network (ECN, `http:\\www.ca.sandia.gov/ecn`) was established, so that it could provide an open forum for international collaborations among experimental and

*Corresponding author. Email: gianluca.derrico@polimi.it

computational researchers in engine combustion. The current state of the art of this project includes a series of constant-volume diesel combustion experiments under non-reacting and reacting conditions, conducted in parallel in several institutions to guarantee the reproducibility of the observed phenomena [1]. On the modeling point of view, different challenges can arise and be matter of investigation. In particular, one of the topics which has seen a renewed interest in the ECN workshops is the capability of correctly describe the ignition process as function of different ambient conditions together with a correct prediction of the lift-off heights [2–6]. There is in fact a general agreement in considering this issue the first requirement to correctly describe the flame structure and the occurring pollutant formation (i.e soot and NO_x) [7]. Discussion is still open and the sharing of well-documented experiments within the ECN network is a great opportunity to perform an extensive comparison among different models.

As recently reviewed in [2], different approaches were successfully applied to describe Diesel spray combustion and the definition of the most suitable model might depend on the occurring combustion mode: homogeneous reactor, diffusion flame or propagating diffusive front regime [8]. Realistic results can be achieved only if both complex fuel chemistry and its interaction with turbulence are properly taken into account. Most of the models that are used for combustion simulations with detailed chemistry are based on flame structure assumptions (equivalent stretched diffusion flame, partially-stirred reactor, homogeneous reactor, ...) and compute the chemical composition or the reaction rate in each computational cell accordingly [9, 10]. Among the available approaches which account for finite rate chemistry, both Representative Interactive Flamelets (RIF) and zero-dimensional Conditional Moment Closure (CMC) operate a coordinate transformation that makes possible to solve the diffusion-reaction problem in the mixture fraction space, assumed to be the predominant variable in non-premixed combustion problems [11, 12]. Effects of local flow are incorporated in the scalar dissipation rate variable and chemical composition is estimated on the basis of a presumed statistical distribution of each chemical species which depends on the mixture fraction and its variance. Within this class of flamelet based approaches, a very popular choice is the use of tabulation of the reaction rates, as for example done in the Unsteady Flamelet Progress Variable (UFPV) model [2] or in the Flamelet Generated Manifold (FGM) method [13, 14], which introduce a reaction progress variable to characterize mixing and progress of combustion.

Alternative interpretations of the flame ignition and flame stabilization mechanism neglect any sub-grid interaction between turbulence and chemistry, assuming each cell to be homogeneous [15]. This approach is particularly suited to describe HCCI and PCCI combustion [16, 17], but in literature there are different examples of applications to Diesel combustion [4, 18] or stratified combustion in spark-ignition, direct-injection engines [20], which show rather good prediction of flame stabilization, auto-ignition time, heat release rate profiles and pollutant emissions trends as long as a fine grid is used.

Over the last years the authors have contributed to the development and application of libraries and solvers for the modelling of i.c. engines based on the multipurpose CFD code OpenFOAM [21], which is fully open-source and written in a highly efficient object-oriented programming. These features allow an easy implementation and testing of different approaches. In the present work, two different combustion models, based on different interpretations of the flame stabilization mechanism, were implemented and tested to reproduce a very popular public domain set of experiments, as the so-called Spray A of the Engine Combustion Network [22]. In the first model, a perfectly strirred reactor(PSR) approach is followed, in which

each cell is assumed to be a homogeneous reactor and the chemical species reaction rates are computed accordingly. To reduce the computational time due to the use of complex chemistry, a multi-zone approach, called CCM (Chemistry Coordinate Mapping) [23, 24], was developed by the authors and combined with tabulation of dynamic adaptive chemistry (TDAC) [17]. The second model, which was recently implemented by the authors in the same CFD platform, is the so-called mRIF (multiple Representative Interactive Flamelets). It approximates the flame structure as a set of multiple unsteady laminar diffusion flames (*flamelets*), whose evolution is computed in the mixture fraction space [11] where species and energy equations are solved. It is remarked that the in the flamemet domain chemistry is integrated by the same ODE solver and TDAC algorithm which are used in the PSR approach. Effects of mixing are incorporated in the scalar dissipation rate, which is computed as a conditional average of its distribution in the CFD domain. Use of multiple flamelets ensures a better prediction of both flame structure and auto-ignition, since spatial variations of the scalar dissipation rate are properly taken into account [26, 27].

The paper is organized as follows. First the two combustion models are presented together with a short description of the used Lagrangian-Euler spray model. Next the studied experiment is described and a baseline non-reacting case is examined, to show the achieved accuracy in terms of liquid and vapor penetration, as well as mixture fraction distribution. Finally different reacting conditions, all taken from the ECN experiments, are simulated with both approaches. The assessment of the two approaches is presented comparing the computed results with the measured data of ignition delay, lift-off, pressure rise and flame location. A discussion of the main differences of the predicted flame structure, described by the species and temperature distribution, by the two approaches concludes this investigation.

2. Numerical methodology

The CFD tool used in the present work is OpenFOAM, together with the Lib-ICE set of solvers and libraries developed by the authors to simulate I.C. engines. The gas phase is described using the URANS formulation and mass, momentum and energy equations are solved for a compressible, multi-component flow using the second-order, unstructured finite-volume method supporting polyhedral cells. The standard $k - \epsilon$ model was used for turbulence. Pressure and velocity equations are coupled by the PIMPLE algorithm, which is a combination of the well-known PISO and SIMPLE techniques [28] and ensures both stability and accuracy. The discrete droplet method (DDM) is used to compute the evolution of the liquid fuel spray, which is assumed to be composed by a set of computational parcels, each one of them representative of identical droplets. Parcels are tracked into the CFD domain in a Lagrangian fashion, exchanging mass, momentum and energy with the gas phase. First-order temporal discretization and implicit second-order schemes were used. Transport properties of each species are evaluated using NASA's polynomial coefficients. Specific sub-models are employed to describe fuel atomization, breakup, heat transfer, evaporation, collision and wall impingement. As previously explained, two different combustion models based on the use of complex chemistry, were used and compared: a well-mixed and an unsteady flamelet approach. In the next sections first a brief overview of the spray-sub models is given and then the two different combustion models which are compared in this work are extensively presented.

2.1 Liquid spray sub-models

Atomization of the liquid fuel jet is predicted by the Huh-Gosman model [29]. Primary parcels (blobs) are injected into the computational mesh with size equal to the nozzle diameter and their velocity is function of the injected mass flow rate profile. Both Kelvin-Helmholtz and turbulence induced breakup on the jet surface are taken into account by the model, describing the diameter reduction of the primary droplets inside each parcel as follows:

$$\frac{dD}{dt} = -C_5 \cdot \frac{L_a}{\tau_a} \tag{1}$$

where C_5 is the main model constant, L_a and τ_a are the characteristic atomization length and time scale. Their values are related to the geometry of the injection system, turbulence decay within the jet and Kelvin-Helmholtz instabilities. At the nozzle exit, the spray angle α is predicted according to the expression:

$$tan\left(\frac{\alpha}{2}\right) = \frac{L_a/\tau_a}{U} \tag{2}$$

where U is the droplet velocity at the nozzle exit. Secondary droplets are created from primary blobs when the when the amount of mass stripped from each parcels, computed to from Eq. 1, is higher than a specific threshold value. Their diameter is computed from a Rosin Rammler distribution, whose maximum value is the nozzle diameter, while the minimum value is computed as follows:

$$d_{min} = 2 \cdot \pi \frac{(\rho_{liq} + \rho_{gas}) \cdot \sigma}{\rho_{liq} \cdot \rho_{gas} \cdot U^2} \tag{3}$$

where σ is the liquid surface tension. The secondary stripped droplets experience only the Kelvin-Helmholtz (*Wave*) breakup [30]. In such case, their diameter reduction is:

$$\frac{dD}{dt} = -\frac{D - D_{new}}{\tau_{bu}} \tag{4}$$

where D_{new} is the diameter of the new child drops, and τ_{bu} is the breakup time:

$$D_{new} = B_0 \cdot \Lambda \tag{5}$$

$$\tau_{bu} = 1.894 \cdot B_1 \cdot \frac{D_{new}}{\Omega \cdot \Lambda} \tag{6}$$

Ω and Λ represent the most unstable growth rate and wave number [30] respectively. The parameter B_0 is set to 0.61 while B_1 should be adjusted to match experimental data of spray penetration. Theoretically, the same approach used for primary atomization should be applied also to secondary breakup. Hence, new child particles should be created because of diameter reduction of secondary droplets. However, to keep an acceptable CPU time, this aspect was neglected since it significantly increase (by an order of magnitude) the total amount of parcels in the CFD domain. Heat transfer between the liquid phase and surrounding gas was modeled by using the Ranz-Marshall correlation, while droplet evaporation rate was computed from droplet size, Spalding and Nusselt numbers [31]. Collision and

coalescence were not taken into account since they have a minimum influence when evaporating sprays have to be simulated [32, 33].

2.2 Combustion model: well-mixed approach

This approach treats each computational cell as a closed homogeneous reactor and computes the chemical species reaction rates accordingly. To this end, an ODE stiff solver takes the thermodynamic conditions (T, p, Y_i) in each cell and integrates the chemical problem within the time-step, solving the species and energy equations. Then species mass fractions are updated as:

$$Y_i^*\left(t+\Delta t\right) = Y_i\left(t\right) + \int_t^{t+\Delta t} \dot{\omega}_i \frac{W_i}{\rho} dt' \tag{7}$$

where ρ is the density, $\dot{\omega}_i$ is the reaction rate and W_i is the molecular weight of the species i. Solution of Eq. 7 is carried out by means of a multi-step, Semi-Implicit Bulirsch-Stoer method, *SIBS* [34].

Finally, the reaction rate $\dot{Y}_i$ is estimated as:

$$\dot{Y}_i = \frac{Y_i^*\left(t+\Delta t\right) - Y_i\left(t\right)}{\Delta t} \tag{8}$$

and it is included in the chemical species transport equations as an additional source term. The main advantage of the well-mixed model is represented by its flexibility with respect to both chemical mechanism and composition of the fuel. Despite it does not account for any sub-grid turbulence-chemistry interaction, such model was successfully applied over the years in a wide range of operating conditions and combustion modes: conventional Diesel and SI, HCCI, PCCI [9, 17, 20]. For what concerns applications to Diesel spray combustion conditions, the model capabilities to predict both flame stabilization and structure were extensively discussed and demonstrated in [3, 4, 15].

2.2.1 Multi-zone Chemistry Coordinate Mapping (CCM)

To integrate the stiff ODEs of elementary reactions and estimate the source term in the species transport and energy equations a recently developed high efficient CCM approach is used. A brief description of the CCM approach is given below. Further information is available in ref. [23–25]. First, a phase space consisting of three principal variables $\tilde{T}$, J_H and $\alpha = \log_{10}(\nabla J_H \cdot \nabla J_H + 1)$ is constructed. J_H is elemental mass fraction of hydrogen atom defined as:

$$J_H = \sum_{k=1}^{N} \frac{W_H}{W_k} \beta_{H,k} \tilde{Y_k}, \tag{9}$$

where W_H and W_k are the atomic and molecular weights of the hydrogen and the $k-$th species, respectively. $\beta_{H,k}$ is the number of H-atom in the $k-$th species. Note that variables α and $\nabla J_H \cdot \nabla J_H$ are uniquely related each other. In ref. [25], it has been shown that fuel mass fraction may also be added to the phase space to account for low-temperature chemistry specially at high level of EGR. In this way computational cells are mapped into a three dimensional (T, ∇J_H, α) space.

Let the phase space be discretized by N_T number of temperature zones, N_J number of J_H zones, and N_α number of α zones. The (i, j, k) cell in the physical

domain is mapped to the (l, m, q) zone in the $(\tilde{T}, J_H, \alpha)$ space. In discretized form the mapping is between the index (i, j, k) of the cells in the physical domain to the index (l, m, q) of the zones in the phase space. For each cell in the physical domain, cell indices, i.e., the value of $i_T(i, j, k)$, $i_J(i, j, k)$, and $i_\alpha(i, j, k)$ in the phase space are stored on line at each time-step during the simulation, and they will be used later for the procedure of mapping back results from the phase space to physical space. The mean values of the variables in the phase space zones are determined and used as the initial condition for integrating the reaction rates. The mean reaction rate is then computed for each zone and mapped back to the cells in the physical space using the stored mapping index. Differently from many of the available multi-zone approaches [35, 36], using only a two-dimensional tabulation that accounts for mixture fraction and temperature, in the CCM approach local flow and mixing conditions are also taken into account through the $\nabla J_H \cdot \nabla J_H$ term. This makes the proposed tabulation method more oriented to the combustion mode that is going to be simulated. Furthermore, the chosen set of tabulation variables (T, ∇J_H, α) is generaly enough to make the CCM approach suitable for simulation of multiple combustion modes such as premixed, non-premixed and also multi-fuel.

2.3 Combustion model: multiple Representative Interactive Flamelets (mRIF)

This model is based on the laminar flamelet concept, assuming that the smallest turbulent time and length scales are much larger than the chemical ones and there exists a locally undisturbed sheet where reactions occur [37]. This sheet can be treated as an ensemble of stretched counter-flow diffusion flames, called *flamelets*. The advantage of such treatment is that the temporal evolution of all reacting scalars only depends on the mixture fraction variable, Z, which is related to the local fuel-to-air ratio for non-premixed combustion. Hence, local chemical composition can be estimated from the Z field in the CFD domain, assuming that its sub-grid distribution can be represented by a β-pdf. To this end, transport equations for both Z and its variance need to be solved, accounting for spray evaporation effects [38]. In this work, the approach proposed by Hasse was followed [39] :

$$\frac{D\left(\rho\tilde{Z}\right)}{Dt} + \nabla \cdot \left(\frac{\mu_t}{Sc_Z}\nabla\tilde{Z}\right) = \dot{S} \tag{10}$$

$$\frac{D\left(\rho\widetilde{Z''^2}\right)}{Dt} + \nabla \cdot \quad \frac{\mu_t}{Sc_{\widetilde{Z''^2}}}\nabla\widetilde{Z''^2}\Bigg) = 2\frac{\mu_t}{Sc_{\widetilde{Z''^2}}}\left|\nabla Z\right|^2 + \alpha_{BY}\left\{2\left[\xi\tilde{Z}^{\xi-1} - (\xi+1)\,\tilde{Z}^{\xi}\right]\right\} - \rho\chi \tag{11}$$

where $\dot{S}$ is the liquid mass evaporation rate per unit volume. Generation of mixture fraction variance is due to strain rate and liquid evaporation. In Eq. 11, the ξ parameter was set to 2 as suggested in [38], while α_{BY} is computed from the following relation which was derived from DNS modeling of spray evaporation in homogeneous turbulence:

$$\dot{S} = \rho \int_{Z=0}^{1} \alpha_{BY} z^{\xi} P(z) dz \tag{12}$$

The sink term appearing in Eq. 11 is the average scalar dissipation rate, which is function of the turbulent time scale and mixture fraction variance:

$$\chi = C_\chi \frac{k}{\varepsilon} \widetilde{Z''^2} \tag{13}$$

where the constant C_χ was set to 2 in this work.

In order to properly account for local flow and turbulence effects on the flame structure and predict flame stabilization, a multiple number of flamelets was used. Each one is representative of a certain portion of the injected fuel mass, and chemical composition in each cell is computed from mixture fraction and flamelet marker distribution as follows:

$$\tilde{Y}_i\left(\vec{x}\right) = \sum_{j=1}^{N_f} M_j \int_0^1 Y_{j,i}\left(Z\right) P\left(Z, \widetilde{Z''^2}\right) dZ \tag{14}$$

For each flamelet marker M_j, the following transport equation is solved:

$$\frac{D\left(\rho \tilde{M}_j\right)}{Dt} + \nabla \cdot \left(\frac{\mu_t}{Sc_Z} \nabla \tilde{M}_j\right) = \dot{S}_{M_j} \tag{15}$$

where the source term $\dot{S}_{M_j}$ corresponds to $\dot{S}$ only for a specified interval of the injection duration, while it is zero elsewhere. In this work, flamelets are sequentially generated and time-intervals were computed by the code in such a way that each flamelet marker contains the same amount of fuel mass. Flamelet markers must also satisfy the following relation:

$$Z = \sum_{j=1}^{N_f} M_j \tag{16}$$

The local flame structure is defined by the flamelet equations that are solved assuming unity Lewis number [40] in the mixture fraction space:

$$\rho \frac{\partial Y_i}{\partial t} = \rho \frac{\chi_z}{2} \frac{\partial^2 Y_i}{\partial Z^2} + \dot{\omega}_i \tag{17}$$

$$\rho \frac{\partial h_s}{\partial t} = \rho \frac{\chi_z}{2} \frac{\partial^2 h_s}{\partial Z^2} + \dot{q}_s + \frac{dp}{dt} \tag{18}$$

where Y_i is the mass fraction of the species i, ρ is the density, Z the mixture fraction, $\dot{\omega}_i$ is the chemical source term of species i, h_s the sensible enthalpy, $\dot{q}_s$ the heat released by the chemical reactions and $\frac{dp}{dt}$ is the average pressure derivative versus time computed in the CFD domain. Eqns. 17 - 18 are solved on a 1-D mesh with the finite volume method. Chemical source terms $\dot{\omega}_i$ were computed at the beginning of each time step, following the same procedure illustrated in Eqns. 7-8. Effects of mixing related to turbulence and flow-field are grouped into the scalar dissipation rate term χ_z expressed as:

$$\chi_z = \widehat{\chi_{st,j}} \frac{f\left(Z\right)}{f\left(Z_{st}\right)} \tag{19}$$

$f(Z)$ has an erfc-profile [41], while scalar dissipation rate at stoichiometric mixture fraction conditions $\widehat{\chi_{st,j}}$ for each flamelet is computed as an average of the local values in each computational cell and accounting for flamelet marker distribution M_j:

$$\widehat{\chi_{st,j}} = \frac{\int_V M_j \chi_{st,l}^{3/2} \rho P(Z_{st})\, dV'}{\int_V M_j \chi_{st,l}^{1/2} \rho P(Z_{st})\, dV'} \tag{20}$$

where P is the β-pdf of the mixture fraction, whose parameters depend on mixture fraction and its variance [39]. In each cell $\chi_{st,l}$ is computed following the Hellstrom formulation [42]:

$$\chi_{st,l} = \frac{\chi}{\int_0^1 \frac{f(Z)}{f(Z_{st})} \tilde{P}(Z)\, dZ} \tag{21}$$

In the mixture fraction space, Eqns. 17 - 18 are initialized with the pure mixing solution. Hence, initial chemical species profiles are computed as:

$$Y_i(Z) = (1 - Z) \cdot Y_{i,air} + Z \cdot Y_{i,fuel} \tag{22}$$

where $Y_{i,air}$ and $Y_{i,fuel}$ represent the species mass fraction on the air and fuel sides, respectively. They are the boundary conditions of Eq. 17 and they are kept fixed for the entire simulation. On the air side only the following chemical species were considered: CO_2, N_2, O_2, H_2O, and initialized according to the simulated conditions. On the fuel side, $Y_{i,fuel} = 0$ for all the species except fuel.

The same procedure was used to initialize the temperature. On the air side, it is computed as the average of the computational domain temperature. For each flamelet enthalpy distribution is then initialized as follows:

$$h_s(Z) = (1 - Z) \cdot h_s(T_{air}) + Z \cdot h_s(T_{fuel}) \tag{23}$$

and temperature in the Z-space is estimated from local enthalpy and chemical composition. While temperature on the fuel side is kept fixed during the simulation, temperature on the air side varies according to the $\frac{dp}{dt}$ term. When a new flamelet is created, the computed species and enthalpy profiles are inherited from the previous one, following the approach proposed by [26].

Fig. 1 summarizes the operation of the mRIF combustion model, illustrating the mutual interactions between the CFD and flamelets domains. At each time-step, average stoichiometric scalar dissipation rate values are passed to each flamelet, that solves Eqn. 17-18 for each flamelet accordingly and computes the chemical composition in the mixture fraction domain $\tilde{Y}_{i,j}$. The chemical composition in the CFD domain is computed from the mixture fraction, its variance and the flamelet marker distributions, according to Eq. 14. PDF integration is performed on-line, at each time-step and for each flamelet. Since the flamelet equations are solved on a 1D mesh with the finite volume method representing the mixture fraction space, integrals are discretized as follows:

$$\tilde{\phi}(Z, \vec{x}) = \sum_{i=1}^{N_{cells}} \tilde{\phi}(Z_i)\, P_Z(Z_i)\, \Delta Z_i \tag{24}$$

where N_{cells} is the number of cells used to discretize the mixture fraction space, and ΔZ_i the cell mesh size. Computational overheads induced by PDF integration are strictly related to the number of flamelets used and CFD mesh size. In general, approximately 20-70% of the CPU time is spent in PDF integration. Temperature is updated from new chemical composition and total enthalpy, whose variation is only due to flow and spray evaporation. For what concerns the simulation setup, the chosen number of flamelet is very important since it mainly determines the flame structure. For each injection event, a total number of 10-30 flamelets seems to be sufficient to properly predict auto-ignition and lift-off. For further information, the reader is referred to [26].

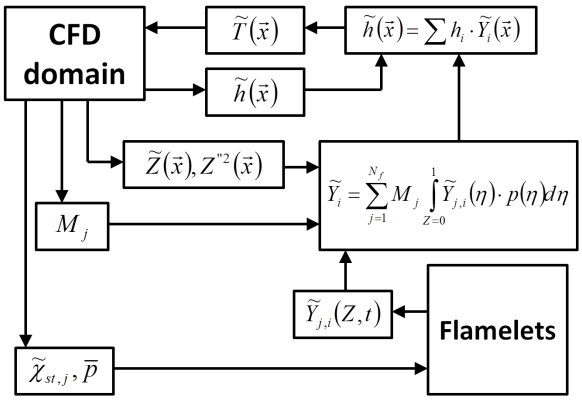

Figure 1. Operation of mRIF model: interaction between flamelets and CFD domain

2.4 Tabulation of dynamic adaptive chemistry

When detailed chemistry is incorporated in combustion models, it is necessary to consider that chemical time-scales are much smaller (2-4 orders of magnitude) than the CFD time-step that is generally used ($10^{-7} - 10^{-5}$). For this reason, ODE stiff solvers need to be employed to properly compute the chemical species reaction rates that are used in the chemical species transport equations, as shown in Eqns. 7,8,17. However, operation of ODE solvers significantly increase the computational time since it involves sub-cycling and computations of large jacobians. Hence, the sizes of mechanisms employed in practical simulations are generally limited to 50 species and 100 reactions [43–45] with a consequent lack in terms of accuracy mainly when advanced combustion modes, high EGR conditions and soot formation processes need to be predicted. To make the use of more detailed mechanisms possible (up to 150 species for Diesel combustion) in a reasonable amount of time, the TDAC algorithm [17–19] was employed in this work that combines the ISAT and DAC techniques [46–48].

The ISAT algorithm intends to reuse computationally demanding results, e.g. the integration of large and stiff ODE systems, by storing those results and all the necessary data to retrieve them. During computation, given a query point, ψ^q, it computes a linear approximation of the mapping:

$$\mathbf{R}(\psi^q) \approx \mathbf{R}^l(\psi^q) = \mathbf{R}(\psi^0) + \delta\mathbf{R}^l \ , \tag{25}$$

where $\delta\mathbf{R}^l = \mathbf{A}(\psi^0)(\psi^q - \psi^0)$ and $\mathbf{A}$ is the mapping gradient matrix defined by

$$A_{ij}(\psi^0) = \frac{\partial R_i(\psi^0)}{\partial \psi_j} \ . \tag{26}$$

The linear approximation defined by Eq. 25 is valid in the region of accuracy (ROA) where the following condition is respected:

$$|\mathbf{R}(\psi^q) - \mathbf{R}^l(\psi^q)| = |\delta\mathbf{R} - \delta\mathbf{R}^l| \leq \varepsilon_{\text{ISAT}} \ , \tag{27}$$

where $\varepsilon_{\text{ISAT}}$ is a user-defined tolerance and $\delta\mathbf{R} = \mathbf{R}(\psi^q) - \mathbf{R}(\psi^0)$. In practice, this region is not computed since it would require to compute all the possible mapping $\mathbf{R}(\psi^q)$. Therefore, a conservative hyper-ellipsoid of accuracy is used instead in the composition space to approximate this region of accuracy.

During the calculation, the table is built up according to the received queries. It consists of a binary tree with leafs and nodes. The leafs store ψ, $\mathbf{R}(\psi)$, $\mathbf{A}(\psi)$ and the ROA description. The nodes contain the rules that allow to scan the binary tree to retrieve the appropriate point [46]. The maximum size of the binary tree should be mainly determined taking into account two different aspects: computer memory size and efficiency of the binary tree search algorithm. A maximum size of 10^3 - 10^4 points is suggested resulting from experience of past works [17, 18]. When the maximum number of points is reached, the binary tree is fully cleaned and filled again.

The DAC method computes reduced mechanisms that are valid for the local thermochemical conditions. In this work, DAC has been extended to full CFD meshes with wall heat transfer. The reduction algorithm is executed before every call to the stiff solver to identify the relevant species and reactions according to the thermodynamic conditions in each cell [47, 48].

The coupling of ISAT and DAC performed in this work is schematically illustrated in Figure 2. When ISAT receives a query ψ^q that needs to integrate the ODE set, it provides ψ^q to the DAC algorithm which then finds the reduced mechanism for the local thermochemical conditions and provides the reduced set of active species ψ^q_a to the ODE solver. This solver computes the reaction mapping for the reduced set $\mathrm{R}(\psi^q_a)$ that is used by ISAT to build the reaction mapping $\mathrm{R}(\psi^q)$ in the full composition space. This is performed by using the $\mathbf{A}$ matrix in the reduced system and by adding the initial concentration of the disabled species.

Using simplification methods at distinct levels combines their effects and allows a significant reduction of the computational cost. The use of TDAC ensures speed-up factors ranging from 10 to 1500 depending on the mechanism size and simulated combustion mode [17, 18]. The TDAC tecnique was used for both the well-mixed and unsteady flamelet approach.

3. Results and discussion

Experiments conducted within the Engine Combustion Network [1], `http://www.ca.sandia.gov/ecn`, in a constant-volume chamber were used to assess the potentialities and limits of the two combustion models to describe a turbulent spray flame. In the present study both non-reacting and reacting conditions in which dodecane ($C_{12}H_{26}$) was employed as fuel were considered.

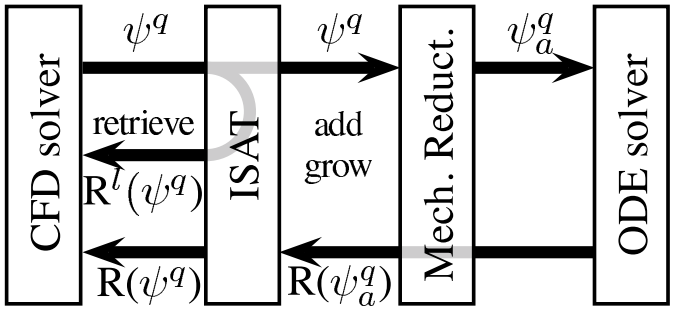

Figure 2. TDAC: combination of ISAT and DAC

3.1 Non reacting condtions

In a previuos investingation [33] the authors extensively discussed the capabilities of the proposed Eulerian-Langrangian approach to correctly describe the liquid and vapor spray distribution under non-reacting conditions considering the entire 3D domain. The well known dependencies of the results on the choice of the numerical scheme, time step, mesh size and spray sub-model constants were assessed, leading to the definition of a best practice methodology. Since in the present work attention is mainly focused on the simulations under reacting conditions, conclusions and guidelines from previous works were taken and applied to a 2D axisymmetric geometry in order to reduce the computation effort. A summary of the employed numerical set-up (e.g., mesh size and distribution, computational time step, numerical schemes, spray-submodel costants) is given in Table 1.

Table 1. Main data of model choice and set-up

Mesh type	2D
Minimum mesh size	0.1 mm
time step	0.25 ms
Atomization model C_5	Huh-Gosman XX
Breakup model B_1	KH (wave) XX
Turbulence model	$k-\varepsilon$
Spatial discretizatoin	2^{nd} order
Temporal discretizatoin	1^{st} order

Two conditions were selected among the available database of non-reacting conditions on the basis of the similarity with the reacting conditions which will be matter of investigation. They respectively correspond to an ambient gas density of 22.8 kg/m^3 and 15.2 kg/m^3 and an ambient temperature of 900 K and 1100 K. Figures 3(a)-(b) compare the measured and computed liquid and vapor penetrations, evidencing a good agreement between the two set of data.

This comparison does not give any quantitative assessment of the fuel-air distribution, which is of course the fundamental prerequisite for any combustion simulation. However for these two conditions Rayleigh scattering measurements were performed for fully developed spray. Figures 4(a)-(b) compare the radial distributions of mixture fraction Z and its variance $\widetilde{Z''^2}$ at two axial positions (25 mm and 45 mm from the injector nozzle) at 1.5 ms ASI, while Figure 5 compares the axial mixture fraction distribution at the same time.

It is evident that the simulations are able to capture not only qualitatively but also quantitatively the fuel-air distribution under steady conditions (1.5 ms ASI). Unfortunately a similar validation under transient conditions was not possible because of the lack of such measured data. However the achievement of a such accu-

racy under steady conditions for the mixture fraction distributions together with the good description of the transient vapor penetration, as shown in Figures 3(b), constitute already an adequate validation to be able to proceed to the simulation of the reacting conditions. For what concerns prediction of mixture fraction variance, maximum $\widetilde{Z''^2}$ values are located approximately 2 mm radial distance from the injector axis. Computed results are in fair agreement at 25 mm axial distance (Fig. 4(a)), while at 45 mm axial distance (Fig. 4(b)) location of maximum $\widetilde{Z''^2}$ is much closer to the injector axis compared to the experimental profile, despite the maximum value is correctly predicted. Possible reasons for this discrepancy might be related to the mesh size and and turbulence model used in this work.

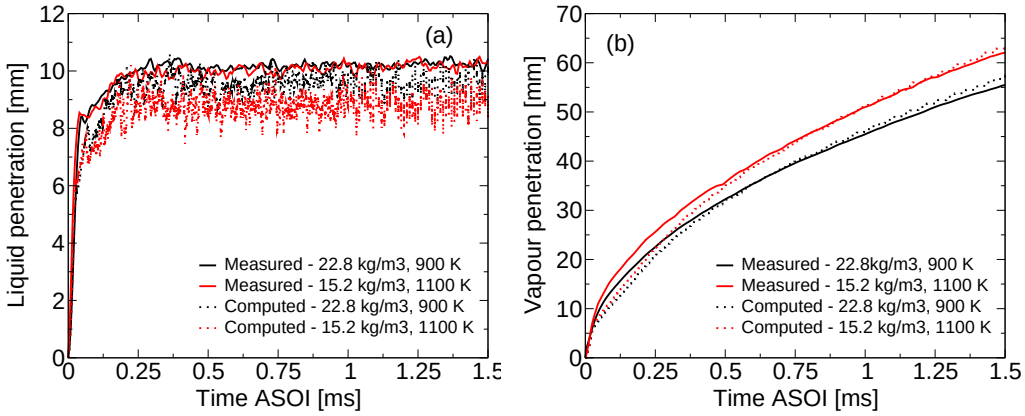

Figure 3. Measured and computed liquid (a) and vapor (b) penetrations for two different ambient initial conditions.

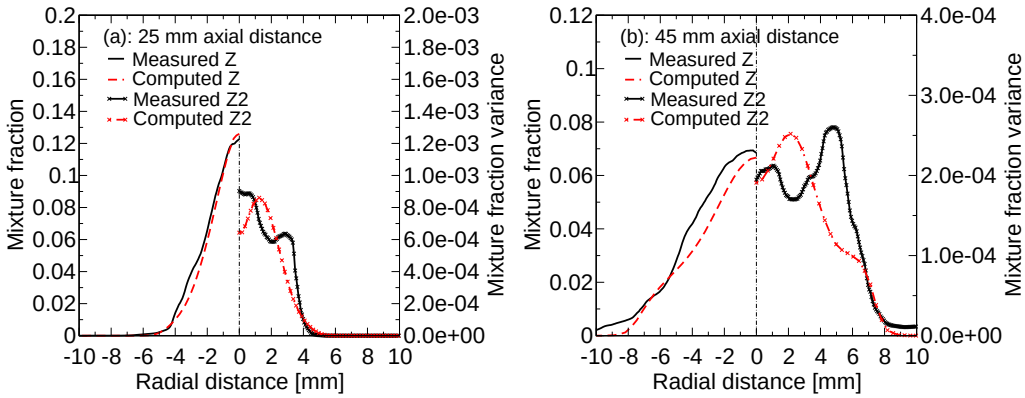

Figure 4. Comparison between experimental and computed radial mixture fraction distribution (left panel) and its variance (right panel) at 25 mm (a) and at 45 mm (b) from the injector.

3.2 Reacting conditions

Validation and comparison of the combustion models for the reacting conditions were performed following the guidelines defined within the Engine Combustion Network. The chosen skeletal detailed reaction mechanism for n-dodecane-air consists of 106 species and 420 reactions [49]. Its size can be considered acceptable for a CFD computation of diesel spray combustion not only in the present investigation but eventually for the description of the combustion process in a Diesel engine geometry too. Before proceeding with its application to the ECN test cases

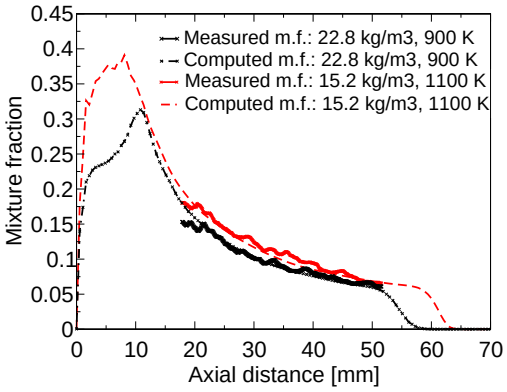

Figure 5. Comparison between experimental and computed axial mixture fraction distribution.

together with the afore described combustion models, the feasibility of this skeletal reaction mechanism was validated by comparing the autoignition delay times for premixed n-dodecane/air mixtures with shock tube experimental data [50]. Of course this investigation had already been carried our by the authors of the skeletal mechanism, but here it was repeated using OpenFOAM and its ODE solver to verify the consistency of the numerical results in the CFD platform used in the present study. In the simulations, homogeneous, adiabatic conditions with constant internal energy constraint (constant u) were imposed, while experimental ignition delay times were measured behind reflected shock waves using a high-purity, high-pressure shock tube (HPST) [50]. Figure 6 shows this comparison for ignition delay times for n-dodecane/air for $\phi = 1$ and $\phi = 0.5$. Results are consistent with the ones obtained by Som et al. [49] and similar to the ones obtained with other and more detailed mechanisms [51]. However, an overestimation of the ignition delay times at high temperature until 950 K and an underestimation from 900 K to 800 K can be observed.

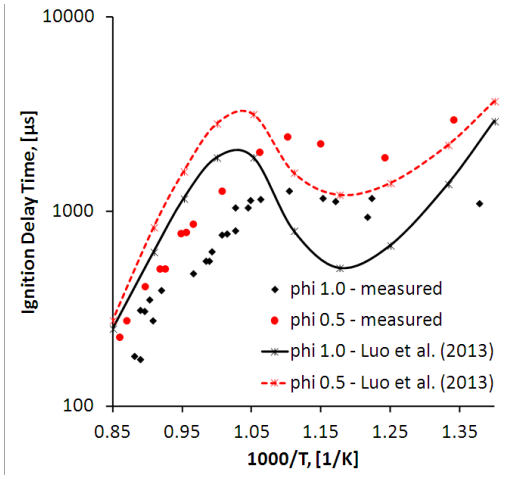

Figure 6. Comparison between measured ignition delay times in n-dodecane/air shock tube experiments [50] and computed values in OpenFOAM useing the Som at al. [49] reduced kinetic mechanism.

Hence, the reacting cases which were defined as target conditions within the Engine Combustion Network were considered. Here one operating condition was chosen as baseline, which was intended to represent a low-temperature combustion regime for modern engines. Specifically, it represents a low-temperature, lower-effective-compression-ratio combustion using EGR and intake pressure boost (do-

decane as fuel, ambient gas initial conditions: temperature 900 K, pressure 60 bar, density 22.8 kg/m^3, oxygen concentration 15%). Hence parametric variations of the operating conditions (ambient temperature, oxygen concentration, fuel pressure) were defined and tested experimentally. Pressure-based ignition delays were recorded together with flame lift-off measurements obtained by OH chemiluminescence [7, 52]. Numerically ignition delay was defined as the time from the start of injection to the time where the maximum temperature rise happens, while the lift-off length (LOL) was defined as the axial distance from the injector where the OH mass fraction reaches 2% of its steady-state maximum value. These definitions were both suggested from the Engine Combustion Network. The influence of ambient temperature and oxygen concentration was assessed in this study, considering five different temperatures (800 K, 900 K, 1000 K, 1100 K, 1200 K) at constant density (22.8 kg/m^3) and oxygen concentration (15%) and three different oxygen concentrations (13%, 15%, 21%) at constant temperature (900 K) and constant density (22.8 kg/m^3).

Figure 7(a) shows the comparison between measured and computed axial ignition delay as function of the ambient temperature for both the well-mixed combustion model and the multiple representative interactive flamelet (mRIF) approach. For the latter, 1 flamelet was introduced every 0.1 ms from the start of injection. Of course the definition of the number of flamelets is critical and may partially influence the flame development and structure. This aspect is not included as matter of discussion in the present study, but this choice has been done after conducting an extensive sensitivity analysis of the results on the number of flamelets. Computed results are very similar in terms of prediction of the ignition delay. Both approaches tend to overestimate the onset of high temperature reactions with respect to the experiments, but the overall trend is in agreement with the measured values. Similarly Figure 7(b) shows the corresponding comparison between measured and computed lift-off length as function of the ambient temperature. In this case the mRIF model quantitatively exhibits better results than the well-mixed method compared to the experimental findings, apart from the condition at higher temperature (1200 K) where the unsteady flamelets approach significantly underestimates the flame lift-off. Of course there are several interacting factors behind such results and to help a deeper understanding of the observed similarities and differences, the transient flame structures predicted with the two models for the baseline condition (900 K) are analyzed here in detail.

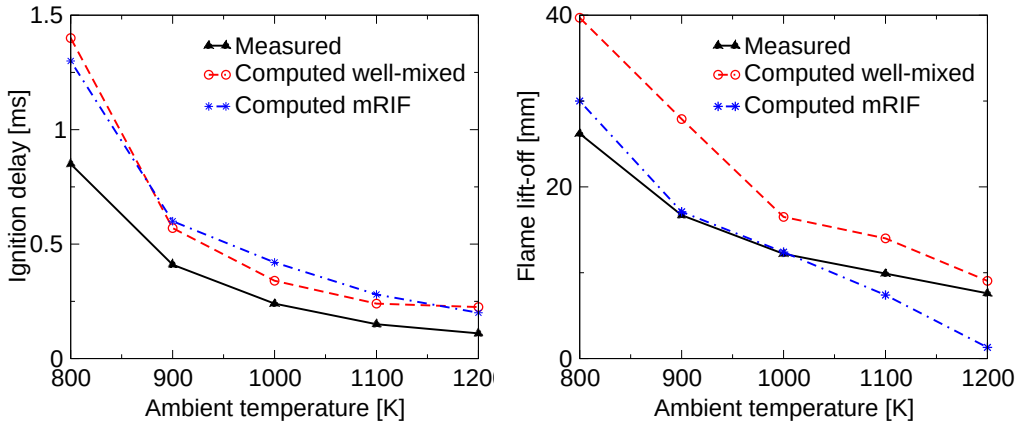

(a) Ignition delay

(b) Flame lift-off

Figure 7. Comparison between measured and computed axial ignition delay (a) and flame lift-off (b) as function of the ambient temperature at 20 bar ambient pressure.

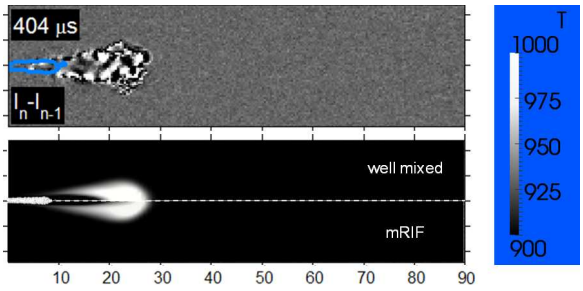

Figure 8. Schlieren image and computed temperature distribution at 0.4 ms with the well-mixed (upper half) and mRIF (lower half) models.

On the experimental side, different diagnostic techniques such as high-speed schlieren, Mie-scatter, and chemiluminescence imaging were used in the different institutions involved in the ECN framework to characterize both the spray and the flame. For the scopes of the present investigation, the first relevant optical acquisition is the one just before high temperature combustion occurs. This corresponds to 0.4 ms, time at which a cool flame was observed to be fully developed. Figure 8 shows in the upper part the Schlieren acquisition, with image pairs shown with raw schlieren and also with background correction from successive images in order to more easily visualize the actual jet structure, as opposed to background schlieren. Liquid border are marked in blue. The lower part of Figure 8 shows the temperature distributions computed with the well-mixed and with the multiple representative flamelet (mRIF) model. The computed distributions are rather similar with a more extended reacting zone in the well-mixed model and, even if a quantitative assessment is not possible, the agreement with the optical image seems rather good in both cases. To further help the understanding of the occurring processes, in Figure 9 the scattered temperature distribution of the well-mixed model and the solutions for the first four flamelets in the temperature-mixture fraction space for the mRIF model at 0.4 ms are compared.

In both models, low temperatures reactions are taking place in the rich mixture around $\phi = 1.2$, which then corresponds to the visible part of the flame in Figure 8. The use of multiple flamelets allows to describe in detail the different stages of the ignition process in the computational domain: the fourth flamelet is experiencing a cool flame, while the other ones are almost in their main ignition. Results in the unsteady flamelet approach depend not only on the air-fuel mixing and on the chemistry, but also on the evolution of the scalar dissipation rate (SDR). In a Diesel jet the SDR will initially be very high for the first injected drop and then decreases as the mixture field homogenizes. However, as already shown in previous works [27], the time-scale of the cool flame is rather independent of scalar dissipation rate (as long as it is lower than the quenching value), therefore the two model have a similar flame structure during the development of these low-temperature reactions.

Then, ignition was experimentally detected at 0.41 ms. The Schlieren images show that the flame stabilizes between 15-20 mm shortly after autoignition and the lift-off length remains in this position during the rest of the injection [52]. Figure 10 qualitatively compares the measured chemiluminescence (450-nm short-pass filter, 197 μs exposure duration) at 0.7 ms and at 1.5 ms with the computed temperature distributions. The blue line marks the flame border to locate lift-off. The threshold was experimentally defined as 50% of the chemiluminescence leveling-off value and numerically as the iso-surface where OH mass fraction reaches 2% of the maximum in the domain.

This qualitative comparison evidences that at 0.7 ms the flame tip position is

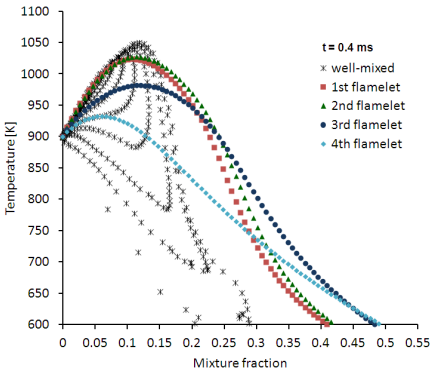

Figure 9. Scattered temperature distribution of the well-mixed model and solutions for the first four flamelets in the T-Z space at 0.4 ms.

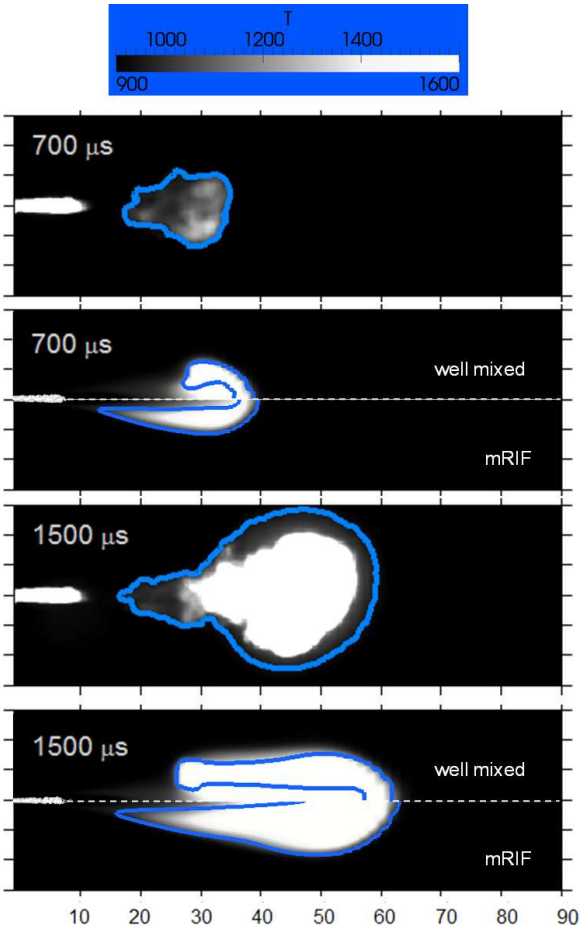

Figure 10. Measured chemiluminescence and computed temperature distribution at 0.8 ms. Measured luminosity and computed (2% of OH_{max}) flame border overlaid.

correct in both models, while the well-mixed model overestimates the lift-off height and the multiple RIF underestimates it. The two approaches in fact, using the same chemistry, predict a similar position of the most reactive sites and of the location of the initial high temperature reactions. In the well-mixed model, each cell is assumed to behave as homogeneous reactor and any sub-grid interaction between turbulence and chemistry is neglected. Hence, after auto-ignition flame propagation will be mainly driven by turbulent diffusion and local flow conditions.

To understand how flame propagation and stabilization are computed by the

mRIF model, both scalar dissipation rate and temperature evolution in the mixture fraction space were analyzed. Figures 11 (a) - (b) report the computed average stoichiometric scalar dissipation rate in the CFD domain and the temperature profiles at stoichiometic mixture fraction Z_{st} for three different flamelets: 1, 3 and 6. As soon as it is created, the flamelet experiences very high scalar dissipation rates, above the extinction limit, that are induced by high velocities and mixture fraction gradients existing close to the nozzle. As soon as the extinction limit is overcome, a cool flame is established approximately after 0.1 ms and then, depending on scalar dissipation rate value and operating condition (ambient pressure and temperature) main ignition takes place [27] afterwards. Despite initialized with the solution from the previous flamelet, it is possible to see that temperature history at stoichoimetric mixture fraction for flamelets 3 and 6 is very similar to the one of the first flamelet. This means that the proposed setup in terms of number of flamelets is fine enough to ensure an independent temperature history to each of them and to properly account for local variations of scalar dissipation rates on flame structure. Since any new flamelet requires a certain amount of time to auto-ignite, the MRIF model is also able to properly reproduce flame stabilization (lift-off), whose generating mechanism is mainly represented by auto-ignition of a diffusion flame. In case only one flamelet was used, a proper prediction of flame stabilization was not possible since after ignition delay temperature distribution would be only function of the mixture fraction, with the lift-off position approximately found at the closer distance from the injector where stoichiometric mixture fraction was found.

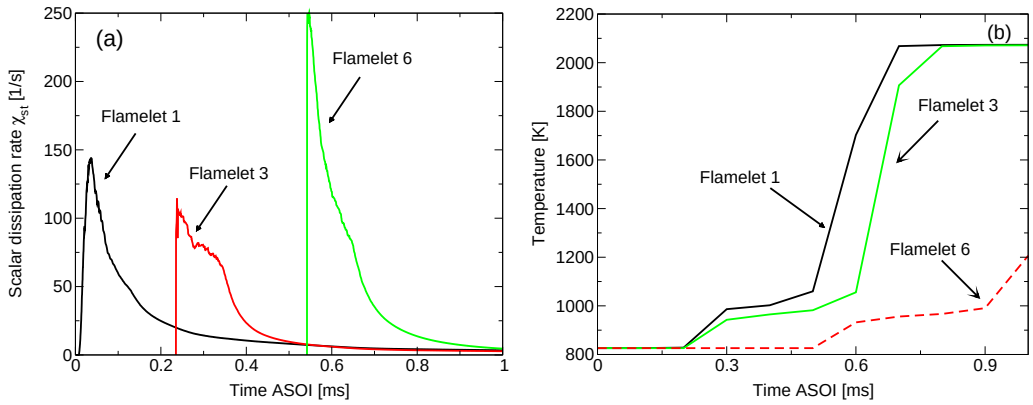

Figure 11. (a) Computed evolution of stoichiometric scalar dissipation rate χ_{st} for flamelets 1, 3, 6; (b) Computed temperature evolution at stoichiometric mixture fraction Z_{st} for flamelets 1, 3, 6.

If we look at the computed solutions in the temperature-mixture fraction space at 0.7 ms, i.e. Figure 12, we noticed that in both models high temperature reactions are taking place near the stoichiometric mixture, where the first two flamelets have reached a quasi-steady state which correspond to the scattered higher temperatures of the well-mixed approach.

At 1.5 ms the flame has reached a steady state position for this operating condition. The lower part of Figure 10 shows the qualitative comparison between the measured chemiluminescence and the computed temperature distributions. Both approaches well capture the position and extension of the region of higher temperature and luminosity, while the multiple RIF approach is in better agreement with the chemiluminescence imaging for the definition of the lift-off height.

Unfortunately a further quantitative assesment is not possible, but it is considered equally important to compare in detail the flame structure computed by the two approaches at the steady state condition. Figures 13(a)-(b) show the computed temperature and OH distributions at 1.5 ms with the well-mixed combustion and

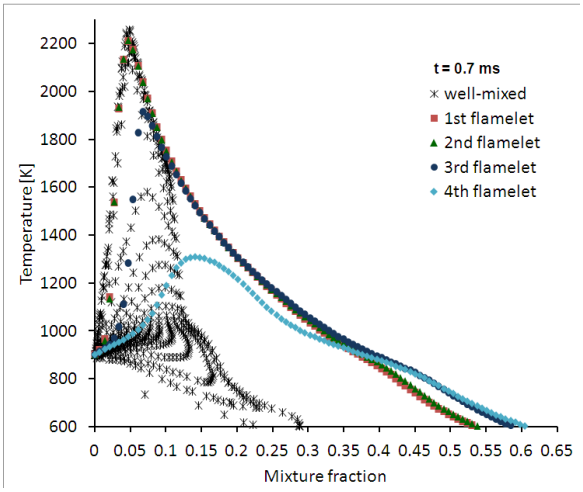

Figure 12. Scattered temperature distribution of the well-mixed model and solutions for the first four flamelets in the T-Z space at 0.7 ms.

multiple RIF model respectively. The comparison of the OH distributions evidences a broader region and lower peak mean values for the mRIF model than the well-mixed model, whose OH profile is rather thin. This difference is due the different description of the mixing rate which is related to the strain rate as known in the flamelet approach. These findings are similar to the ones obtained with other non-premixed turbulent combustion models in which turbulence-chemistry interaction is taken into account [2, 5, 53].

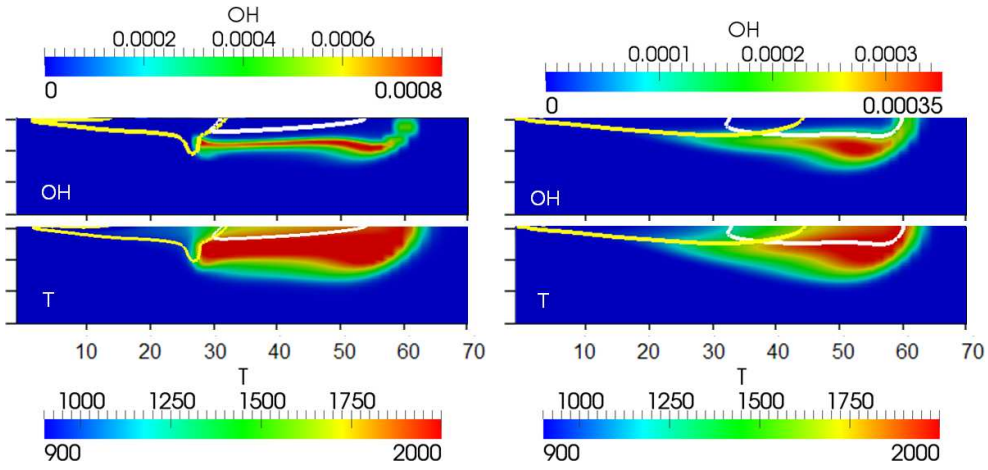

(a) Well-mixed (b) mRIF

Figure 13. Computed temperature and OH distributions at 1.5 ms with the well-mixed (a) and mRIF (b) combustion models. HO_2 and C_2H_2 region are marked with the yellow and white line respectively

In both figures the yellow lines mark the region in which HO_2 exist. This radical in fact plays an important role in the initialization of the high temperature reactions. The analysis of its location in Figure 13(a) evidences once again how in the well-mixed model flame stabilization is entirely achieved by auto-ignition, so that there is almost no overlaid with the flame and the HO_2 further border corresponds to the lift-off height. This condition is obviously not true for the mRIF model, where the flame is stabilized with a different mechanism. Additionally the white line shows the region where a significant concentration of acetylene, C_2H_2, was numerically observed. In both models, these soot precursors are formed in the centre

of the jet, where the mixture is richer. However the acetylene zone has a wider extension in the mRIF model, while it is clearly separeted by the region where OH is formed in the well-mixed approach. On the basis of these considerations, the meaning of the comparison of the lift-off height as function of the ambient temperature, previously shown in Figure 7(b), is more clear and the occurence of differences in the prediction of the lift-off by the two models, being similar the ignition delay time is explained.

A good prediction of the heat release rate during mixing controlled combustion is a fundamental pre-requisite for a proper prediction of the engine efficiency and NO_x emissions. For this reason, to have a quantitative assessment of the capability of each model to predict the burning rate, the measured pressure rises were compared with the computed ones in Figures 14(a)-(b). For any tested condition, neglection of turbulence-chemistry interaction is responsible for a higher burning rate predicted by the well-mixed model compared to mRIF, whose results are in rather good agreement with experimental data. This is particularly clear at 900, 1000 and 1200 K ambient temperatures, representing the three conditions where turbulence-chemistry interaction play a significant role in the combustion development. Results at 800 K are strongly affected by a significant overestimation of the ignition delay, with main ignition predicted after the end of injection. Under this condition, very similar heat release rates are predicted for both well-mixed and mRIF model, and this aspect might suggest the use of well-mixed model when when CI pre-mixed combustion modes, like PCCI, PPC, RCCI, are to be studied.

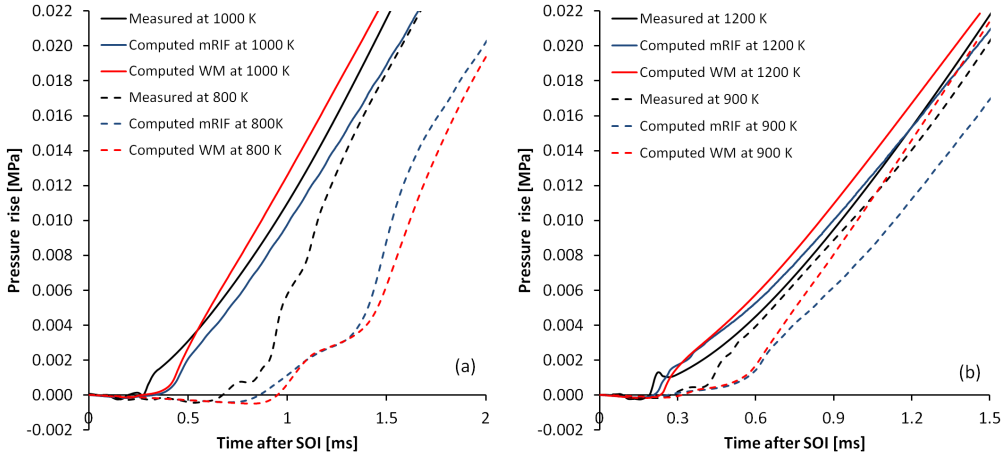

Figure 14. Comparison of measured and computed pressure rise as function of time for different initial air temperature with 15% of O_2.

Effects of ambient oxygen concentrations at 900 K ambient temperature are finally summarized in Figs. 15(a)-(b), where experimental data of ignition delay and flame lift-off are compared with results computed by the well-mixed and mRIF model. A very similar trend was achieved compared to what was found for ambient temperature dependency. Very similar ignition delay values were found for both the models, but the way flame stabilization is predicted by both models lead to different lift-off values, with a rather good agreement achieved when the mRIF model is used.

4. Conclusions

Purpose of this work was to compare in detail two different multi-dimensional models for Diesel combustion based on detailed chemistry using constant-volume

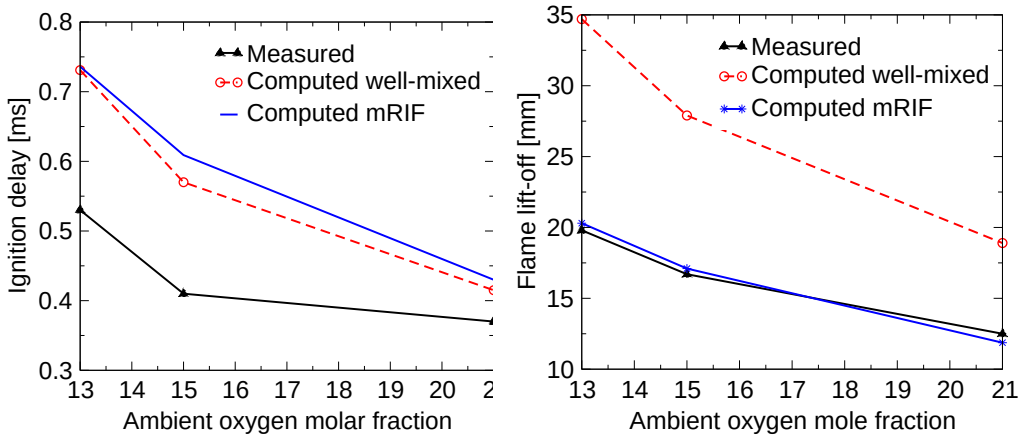

(a) Ignition delay (b) Flame lift-off

Figure 15. Comparison between measured and computed axial ignition delay (a) and flame lift-off (b) as function of the ambient oxygen concentration. Ambient temperature: 900 K.

experiments. The first model is based on the well-stirred reactor assumption, while the second one employs a multiple number of flamelets to describe the diffusion flame originating from auto-ignition of the diesel spray. Both the models were implemented by the authors into an open-source code, together with suitable algorithms for on-line tabulation of reaction rates and mechanism reduction. This made possible to employ a mechanism with 106 species and 420 reactions. Simulations were carried out at different ambient conditions, including both variations of oxygen concentration and ambient temperature.

A detailed comparison between computed and experimental data of ignition delay, flame lift-off and flame structure allowed to understand the differences between the two analyzed approaches. For what concerns the well-mixed model, all the development of the flame depends only on local flow conditions, turbulent viscosity, mixture fraction distribution and chemical mechanism. Which means that, in all cases where liquid spray penetration is significantly lower than vapor penetration (small diameter nozzles, high injection pressures) the well mixed model is capable to properly predict ignition delay with a rather good accuracy, since ignition is going to take place where scalar dissipation rate is very low and homogeneous mixture assumption can be considered correct. However, the two main drawbacks of the well-mixed model seem to be related to the prediction of the burning rate and the flame lift-off. Neglection of turbulence-chemistry interaction makes the flame very thin and causes an overestimation of the heat release rate. Hence, the well-mixed model cannot be, in principle, successfully applied to simulate conventional diesel combustion (even with multiple injections), since it will always overestimate the in-cylinder pressure with negative consequences on the estimated soot and NO_x emissions. Furthermore, the well-mixed model appears to be more sensitive to the chemical mechanism , due to the strong effects of local flow and turbulence on ignition and stabilization. The use of a flamelet based model seems to be more appropriate and prediction of flame lift-off is possible if a multiple number of flamelets is employed. Results with the mRIF model are satisfactory for the entire set of tested conditions both in terms of auto-ignition, flame-lift off and flame structure which is thicker than the one computed with the well mixed model and better agrees with experimental data. According to the mRIF model flame stabilizes because of auto-ignition of a diffusion flame. The validity of such assumption seems to be, however, rather general since at low scalar dissipation rates (long-ignition delay) a sort of premixed auto-ignition is somehow predicted

by the model. On the other hand, when ignition delay is very short and closer to the liquid region, effects of sub-grid mixing and high scalar dissipation rates on auto-ignition are properly taken into account. When looking at possible ranges of application of both well-mixed and mRIF model to engine combustion, the proposed investigation confirms that the well-mixed model can be successfully applied in all the cases where ignition delay takes place after end of injection, i.e. PCCI or HCCI combustion. Under such modes, assumption of homogeneous reactor is correct and the application of a model which is flexible with respect to the fuel composition and chemical mechanism is of great importance. Simulation of conventional diesel combustion, where a relevant portion of the injected fuel burns during mixing controlled combustion phase requires instead the mRIF model due to its capability to predict flame stabilization and heat release rate over a wide range of ambient temperatures and oxygen concentrations. Both of them are fundamental pre-requisite for a proper estimation of in-cylinder pressure and pollutant formation. Possible interaction beween flamelets might need however to be introduced in cases where multiple injections are involved, and this aspect will be objective of a future work.

References

[1] M. Meijer, B. Somers, J. Johnson, J. Naber, S.-Y. Lee, L. M. Malbec, G. Bruneaux, L. M. Pickett, M. Bardi, R. Payri, and T. Bazyn. Engine combustion network (ecn): Characterization and comparison of boundary conditions for different combustion vessels. *Atomization and Sprays*, 22(9):777–806, 2012.

[2] C. Bajaj, M. Ameen, and J. Abraham. Evaluation of an Unsteady Flamelet Progress Variable Model for Autoignition and Flame Lift-Off in Diesel Jets. *Combustion Science and Technology*, 185:pp. 454–472, 2013.

[3] S.C. Kong, Y. Sun, and R. D. Reitz. Modeling Diesel Spray Flame Liftoff, Sooting Tendency, and NO_x Emissions Using Detailed Chemistry With Phenomenological Soot Model. *Journal of Engineering for Gas Turbines and Power*, 129:pp. 245–251, 2007.

[4] S. Som and S.K. Aggarwal. Effects of primary breakup modeling on spray and combustion characteristics of compression ignition engines. *Combustion and Flame*, 157(6):1179 – 1193, 2010.

[5] Y. Pei, E. R. Hawkes, and S. Kook. Transported probability density function modelling of the vapour phase of an n-heptane jet at diesel engine conditions. *Proceedings of the Combustion Institute*, 34(2):3039–3047, 2013.

[6] U. Azimov, K-S. Kim, and C. Bae. Modeling of flame lift-off length in diesel low-temperature combustion with multi-dimensional cfd based on the flame surface density and extinction concept. *Combustion Theory and Modelling*, 14(2):155–175, 2010.

[7] L. M. Pickett and D. L. Siebers. Soot in Diesel Fuel Jets: Effects of Ambient Temperature, Ambient Density and Injection Pressure. *Combustion and Flame*, 138:pp. 114–135, 2004.

[8] V. Mittal, D. J. Cook, and D. Pitsch. An extended multi-regime flamelet model for {IC} engines. *Combustion and Flame*, 159(8):2767 – 2776, 2012.

[9] P. K. Senecal, E. Pomraning, and K. J. Richards. Multidimensional Modelling of Direct-Injection Diesel Spray Liquid Length and Flame Lift-off Length using CFD and Parallel Detailed Chemistry. *SAE Paper*, 2003-01-1043, 2003.

[10] V. Fraioli, C. Beatrice, and M. Lazzaro. Soot particle size modelling in 3d simulations of diesel engine combustion. *Combustion Theory and Modelling*, 15(6):863–892, 2011.

[11] H. Barths, C. Antoni, and N. Peters. Three-Dimensional Simulation of Pollutant Formation in a DI Diesel Engine Using Multiple Interactive Flamelets. *SAE Paper*, 982459, 1998.

[12] Y. M. Wright, G. De Paola, K. Boulouchos, and E. Mastorakos. Diesel engine simulations with multi-dimensional conditional moment closure. *Combustion and flame*, 143(4):402–419, 2005.

[13] C. Bekdemir, L.M.T. Somers, and L.P.H. de Goey. Modeling diesel engine combustion using pressure dependent flamelet generated manifolds. *Proceedings of the Combustion Institute*, 33(2):2887–2894, 2011.

[14] R. Aglave, U. Riedel, and J. Warnatz. Turbulence-chemistry interactions in cfd modelling of diesel engines. *Combustion Theory and Modelling*, 12(2):305–325, 2008.

[15] T. Lucchini, G. D'Errico, D. Ettorre, and G. Ferrari. Numerical investigation of non-reacting and reacting Diesel sprays in constant-volume vessels. *SAE paper*, 2009-01-1971, 2009.

[16] S. Singh, M.P.B. Musculus, and R. D. Reitz. Mixing and flame structures inferred from oh-plif for conventional and low-temperature diesel engine combustion. *Combustion and Flame*, 156(10):1898–1908, 2009.

[17] F. Contino, H. Jeanmart, T. Lucchini, and G.D' Errico. Coupling of in situ adaptive tabulation and dynamic adaptive chemistry: An effective method for solving combustion in engine simulations . *Proceedings of the Combustion Institute*, Vol. 33(2):pp. 3057–3064, 2011.

[18] F. Contino, T. Lucchini, G. D'Errico, C. Duynslaegher, V. Dias, and H. Jeanmart. Simulations of Advanced Combustion Modes Using Detailed Chemistry Combined with Tabulation and Mechanism Reduction Techniques. *SAE Int. J. Engines*, 5:185–196, 2012.

[19] F. Contino, F. Foucher, P. Dagaut, , T. Lucchini, G. D'Errico, C. Mounaim-Rousselle. Experimental and numerical analysis of nitric oxide effect on the ignition of iso-octane in a single cylinder HCCI engine. *Combustion and Flame*, Article in Press, 2013.
[20] X. Yang, A. Solomon, and T. Kuo. Ignition and Combustion Simulations of Spray-Guided SIDI Engine using Arrhenius Combustion with Spark-Energy Deposition Model. *SAE Paper*, 2012-01-0147, 2012.
[21] OpenFOAM website. *http://www.openfoam.org*. The OpenFOAM foundation, 2011.
[22] L. M. Pickett, C. L. Genzale, G. Bruneaux, L.-M L.-M. Malbec, L. Hermant, C. Christiansen, and J. Schramm. Comparison of diesel spray combustion in different high-temperature, high-pressure facilities. *SAE International Journal of Engines*, 3(2):156–181, 2010.
[23] Mehdi Jangi, Tommaso Lucchini, Gianluca D' Errico, and Xue-Song Bai. Effects of egr on the structure and emissions of diesel combustion. *Proceedings of the Combustion Institute*, 34(2):3091 – 3098, 2013.
[24] M. Jangi, R. Yu, and X. S. Bai. A multi-zone chemistry mapping approach for direct numerical simulation of auto-ignition and flame propagation in a constant volume enclosure. *Combustion Theory and Modelling*, 16(2):221–249, 2012.
[25] M. Jangi and X. S. Bai. Multidimensional chemistry coordinate mapping approach for combustion modelling with finite-rate chemistry. *Combustion Theory and Modelling*, 16(6):11091132, 2012.
[26] H. Lehtiniemi, Y. Zhang, R. Rawat, and F. Mauss. Efficient 3-D CFD Combustion Modeling with Transient Flamelet Models. *SAE Paper*, 2008-01-0957, 2008.
[27] H. Barths, C. Hasse, and N. Peters. Computational fluid dynamics modelling of non-premixed combustion in direct injection diesel engines. *International Journal of Engine Research*, 1 (3):pp. 249–267, 2000.
[28] J. H. Ferziger and M. Peric. *Computational Methods for Fluid Dynamics*. Springer, 2002.
[29] K. Y. Huh and A. D. Gosman. A Phenomenological Model of Diesel Spray Atomization. *Proceedings of the International Conference on Multiphase Flows, Tsukuba, Japan*, 1991.
[30] R. D. Reitz. Modeling Atomization Processes In High Pressure Vaporizing Sprays. *Atomization and Spray Technology*, Vol. 3:pp. 309–337, 1987.
[31] W. Ranz and W. Marshall. Evaporation from Drops. *Chemical Engineering Progress*, Vol. 48:pp. 142–180, 1952.
[32] Baumgarten C. *Mixture formation in internal combustion engines*. Springer, 2006.
[33] T. Lucchini, G. D'Errico, and D. Ettorre. Numerical investigation of the spray-mesh-turbulence interactions for high-pressure, evaporating sprays at engine conditions. *International Journal of Heat and Fluid Flow*, 32(1):285–297, 2011.
[34] J. Stoer and F. Bulirsch. *Introduction to Numerical Analysis*. Springer-Verlag, 1980.
[35] M. Raju, M. Wang, M. Dai, W. Piggott, and D. Flowers. Acceleration of Detailed Chemical Kinetics Using Multi-zone Modeling for CFD in Internal Combustion Engine Simulations. *SAE Paper*, 2012-01-0135, 2012.
[36] A. Babajimopoulos, D. N. Assanis, D. L. Flowers, S. M. Aceves, and R. P. Hessel. A fully coupled computational fluid dynamics and multi-zone model with detailed chemical kinetics for the simulation of premixed charge compression ignition engines. *International Journal of Engine Research*, Vol. 6:497–512, 2005.
[37] N. Peters. Laminar Flamelet Concepts in Turbulent Combustion. *21st Symposium on Combustion (Int)*, pages pp. 1231–1250, 1986.
[38] J. Rveillon and L. Vervisch. Spray vaporization in nonpremixed turbulent combustion modeling: a single droplet model. *Combustion and Flame*, 121(12):75 – 90, 2000.
[39] C. Hasse. *A Two-Dimensional Flamelet Model for Multiple Injections in Diesel Engines*. PhD thesis, Technischen Hochschule Aachen, 2004.
[40] H. Pitsch, H. Barths, and N. Peters. Three Dimensional Modeling of NOx and Soot Formation in DI-Diesel Engines Using Detailed Chemistry Based on the Interactive Flamelet Approach. *SAE Paper 962057, SAE Transactions*, 105(4):2010–2025, 1996.
[41] N. Peters. Laminar diffusion flamelet models in non-premixed turbulent combustion. *Progress in Energy and Combustion Science*, 10:319–339, 1984.
[42] T. Hellstrom. RIF implementation and testing. *Technical Report 01.07.1996-31.12.1996*, 1997.
[43] A. Patel, S. C. Kong, and R. D. Reitz. Development and Validation of a Reduced Reaction Mechanism for HCCI Engine Simulations. *SAE Paper*, 2004-01-0558, 2004.
[44] S. Liu, J. C. Hewson, J. H. Chen, and H. Pitsch. Effects of strain rate on high-pressure nonpremixed n-heptane autoignition in counterflow. *Combustion and Flame*, Vol. 137:pp. 320–339, 2004.
[45] S. Tanaka, F. Ayala, and J. C. Keck. A reduced chemical kinetic model for hcci combustion of primary reference fuels in a rapid compression machine. *Combustion and Flame*, 133(4):467–481, 2003.
[46] M.A. Singer and S.B. Pope. Exploiting ISAT to solve the equations of reacting flow. *Combustion Theory and Modelling*, Vol. 8:pp. 361–383, 2004.
[47] Long Liang, John G. Stevens, Sumathy Raman, and John T. Farrell. The use of dynamic adaptive chemistry in combustion simulation of gasoline surrogate fuels. *Combustion and Flame*, 156(7):1493 – 1502, 2009.
[48] Y. Shi, L. Liang, H.-W. Ge, and R. D. Reitz. Acceleration of the chemistry solver for modeling di engine combustion using dynamic adaptive chemistry (dac) schemes. *Combustion Theory and Modelling*, 14(1):69–89, 2010.
[49] S. Som, D.E. Longman, Z. Luo, M. Plomer, and T. Lu. Three Dimensional simulations of diesel sprays using n-dodecane as a surrogate. In *Eastern States Section of the Combustion Institute Fall Technical Meeting*, 2011.
[50] A. Mze-Ahmed, K. Hadj-Ali, P. Dagaut, and G. Dayma. Experimental and modeling study of the oxidation kinetics of n-undecane and n-dodecane in a jet-stirred reactor. *Energy and Fuels*, 26(7):4253–4268, 2012.
[51] C. K. Westbrook, W. J. Pitz, O. Herbinet, H. J. Curran, and E. J. Silke. A comprehensive detailed chemical kinetic reaction mechanism for combustion of n-alkane hydrocarbons from n-octane to n-

hexadecane. *Combustion and Flame*, 156(1):181–199, 2009.
[52] D. L. Siebers and B. Higgins. Flame lift-off on direct-injection diesel sprays under quiescent conditions. *SAE Paper*, 2001-01-0530, 2001.
[53] YM Wright, G De Paola, K Boulouchos, and E Mastorakos. Simulations of spray autoignition and flame establishment with two-dimensional cmc. *Combustion and flame*, 143(4):402–419, 2005.